Journal of Statistical Physics, Vol. 43, Nos. 1/2, 1986

Average Trajectories and Fluctuations from Noisy, Nonlinear Maps

M. Napiórkowski[1,2] and U. Zaus[1]

Received June 13, 1985

The average trajectories and fluctuations around them resulting from an ensemble of noisy, nonlinear maps are analyzed. The bifurcation diagram for the average value obtained from the computer simulation of noisy maps ensemble is discussed first. Then a deterministic average equation of motion describing in an approximate way the time evolution of the average value and of the variance is analyzed numerically. This equation predicts the existence of the bifurcation gap and of the exceptional attractors for special initial points. The scaling properties of the average value and of the variance are obtained with the help of this equation.

KEY WORDS: Noisy nonlinear map; average dynamics; bifurcation gap; transition to chaos; scaling.

1. INTRODUCTION

The influence of external noise on systems governed by nonlinear dynamical laws has recently received much attention.[1–7] One of the basic features of nonlinear systems is their transition to chaotic state as the control parameter is varied. Therefore it is interesting to understand from different points of view how this transition is influenced by the presence of noise. The attemps in this direction are usually based on analysis of a single stochastic equation into which noise is introduced either in an additive or in a multiplicative (parametric) form. In this way the existence of the bifurcation gap was predicted. This means that if in a noise-free case the trans-

[1] Sektion Physik, Universität München, 8000 München 2, Theresienstr. 37, Federal Republic of Germany.

[2] On leave from Institute for Theoretical Physics, Warsaw University, 00-681 Warsaw, Hoża 69, Poland.

0022-4715/86/0400-0349$05.00/0

ition to chaos goes via an infinite sequence of period doublings[8,9] then in the noisy case the chaos sets in after a finite number of period doublings. This number is a decreasing function of the noise strength. In other words the noise blurs the fine details of the bifurcation diagram and makes only a finite number of period doublings observable; the noise strength is a relevant scaling field. The transition to chaos was found to be shifted to smaller values of the control parameter as compared to the noiseless case; it was located by analyzing the Liapunov exponent—as in the noiseless case.

The present approach is different. The average dynamics of noisy maps are studied and quantities averaged over noise histories are analyzed. The reason for this approach is the following. The period-doubling transitions have been observed in many experimental systems[6,10–13] and usually the data are interpreted with the help of simple, nonlinear maps. Then it is natural to include noise in this description. On the other hand the experimentally observed properties of a system are independent of the actual time sequence of random perturbations and this is the reason for studying the average dynamics. The analysis is based on a one-dimensional model with discrete dynamics of the form:

$$x_{n+1} = F(x_n) + \zeta_n \tag{1}$$

where the variable x_n takes values in an interval J and $F(x)$ is unimodal and depends on single control parameter μ. The discussion is restricted to the typical case $F(x) = 1 - \mu x^2$ with $J = [-1, 1]$ and $\mu \in [0, 2]$. We assume that the random impulses ζ_n are independently distributed with $\overline{\zeta_n} = 0$ and $\overline{\zeta_n \zeta_m} = \sigma^2 \cdot \delta_{nm}$, where the parameter σ takes the role of the noise strength.

The value of the variable x at time n calculated from Eq. (1) depends on the starting point x_0 and on the values of noise at all times up to $n-1$: $x_n = x_n(x_0; \zeta_0, ..., \zeta_{n-1})$. According to our program we shall analyze the long-time behavior $(n \to \infty)$ of the average trajectories $\{\bar{x}_n(x_0) \mid n = 0, 1, 2, ...\}$ starting at different initial points; $\bar{x}_n$ denotes the average of $x_n(x_0; \zeta_0, ..., \zeta_{n-1})$ over $\zeta_0, ..., \zeta_{n-1}$. Similarly we shall analyze the fluctuations around these average values, i.e., the variance $\overline{\Delta_n^2} = \overline{x_n^2} - \overline{x_n}^2$ as a function of initial point x_0, control parameter μ, noise strength σ, and time n. The paper is organized as follows. In Section 2 we present the results of computer simulation of an ensemble of noisy maps (1) and discuss the behavior of the average value and of the standard deviation as functions of the control parameter. Then a deterministic average equation of motion is derived. This equation describes in an approximate way the time evolution of the average value and of the variance. It has many interesting and new properties as compared to the noiseless case, i.e., $x_{n+1} = F(x_n)$. They are

discussed in Section 3. In Section 4 the scaling properties of the average value and of the variance are derived on the basis of the average equation of motion. The results are summarized in Section 5.

2. COMPUTER SIMULATION

In this section we discuss the results of computer simulation of an ensemble consisting of 10,000 noisy maps (1). Each variable ζ_n is distributed according to a pseudouniform distribution with the average value $\langle \zeta_n \rangle = 0$ and variance $\langle \zeta_n^2 \rangle = \sigma^2$. The iteration of each noisy map—member of the ensemble—starts at the same initial point x_0 and after each step of iteration the average value and the standard deviation are calculated. The iteration was performed 2200 times, which guaranteed (the exceptions are discussed below) the approach to equilibrium or, in other words, the location of the attractor.

The bifurcation diagram for the average value $\langle x_\infty \rangle$ (Fig. 1) differs

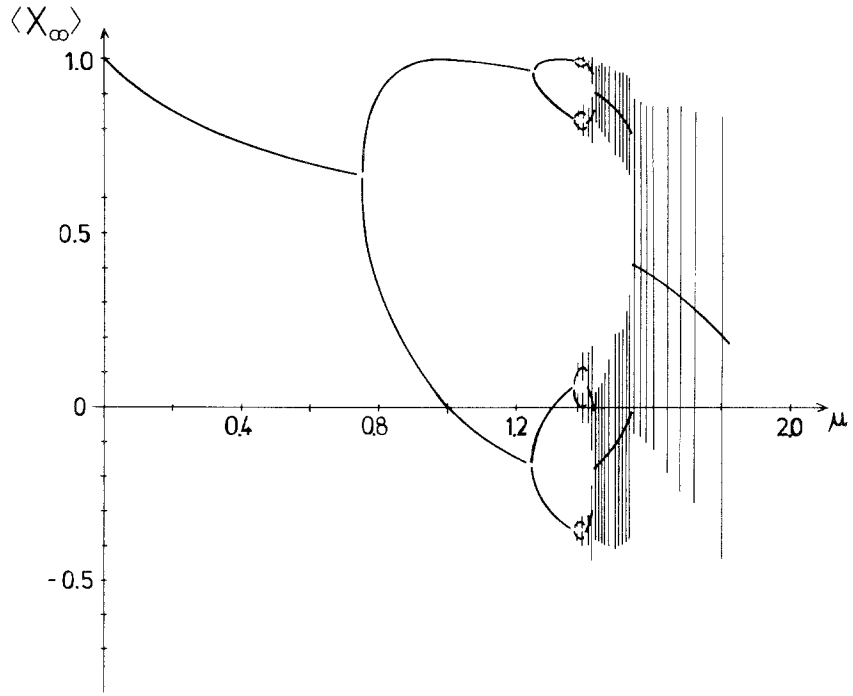

Fig. 1. The bifurcation diagram for the average value $\langle x_\infty \rangle$ obtained from the simulation for noise strength $\sigma = 10^{-3}$. Thin vertical lines denote the standard deviation from the average value for the corresponding μ values. The shifted attractors resulting from the exceptional starting points are not displayed on this diagram.

from the corresponding bifurcation diagram in the noiseless case. First of all, it shows only periodic attractors; there is no chaotic behavior. In the μ regime corresponding to the periodic attractors of the noiseless case, the average attractors are also periodic and undergo the period-doubling transitions. The number of period doublings is finite and depends on the noise strength σ. This number increases with decreasing σ and in the limit $\sigma = 0$ an infinite bifurcation sequence is recovered. For μ in the chaotic regime of the noiseless map again only periodic average attractors are present, and upon increasing μ the inverse sequence of discontinuous mergings of branches of the periodic attractors is observed; for large enough μ an attractor with periodicity one is present. Thus the bifurcation diagram shows certain symmetry with respect to small and large μ values.

It should be stressed, however, that for fixed values of μ and σ the location of the periodic attractor depends significantly on the starting point x_0. This is in contrast with the noiseless case where all points x_0 (except for a set of measure zero) lead to the same attractor.[14] In the average case the overwhelming majority of starting points—we call them the ordinary starting points—lead to an attractor whose location coincides in the periodic μ regime with the location of the corresponding noiseless attractor. The remaining initial points, which are of small but nonzero measure (they are called the exceptional starting points), lead also to periodic attractors which are shifted with respect to the noiseless attractors. The situation for $\mu = 1.36$ and $\sigma = 10^{-3}$ is shown on Figs. 2a, b.

The occurrence of the shifted attractors may be understood as follows: Consider the noiseless map. In the period-q regime the value of its nth iterate $x_n(x_0)$ with $n \gg 1$ will be in the vicinity of one of the branches x_∞^j, $1 \leqslant j \leqslant q$, of the period-$q$ attractor. As x_0 is varied we encounter points $x_0^z(\mu)$ where $x_n(x_0)$ jumps from $x_n(x_0^z - \varepsilon) \cong x_\infty^j$ to $x_n(x_0^z + \varepsilon) \cong x_\infty^k$, $k \neq j$. In the noisy map (1) the effect of ζ_0 is similar to random initial values from an interval of size σ. Hence, if we start to iterate Eq. (1) at some x_0 around x_0^z, the average value $\langle x_n \rangle(x_0)$ will be somewhere between x_∞^j and x_∞^k. In the simulation we find indeed that the intervals of exceptional starting points leading to shifted attractors are centered at the points $x_0^z(\mu)$.

The noise-induced averaging over trajectories starting at neighboring initial points is also responsible for the appearance of periodic attractors at those μ values at which in the noiseless case there are chaotic attractors consisting of separate bands. In this μ regime each branch of the periodic average attractor results from the noise-induced averaging over the corresponding band of the noiseless chaotic attractor. This mechanism is also responsible for the discontinuous mergings of the periodic average attractors around these μ values at which in the noiseless case the phenomenon of band mergings is observed. The fact that for μ values very

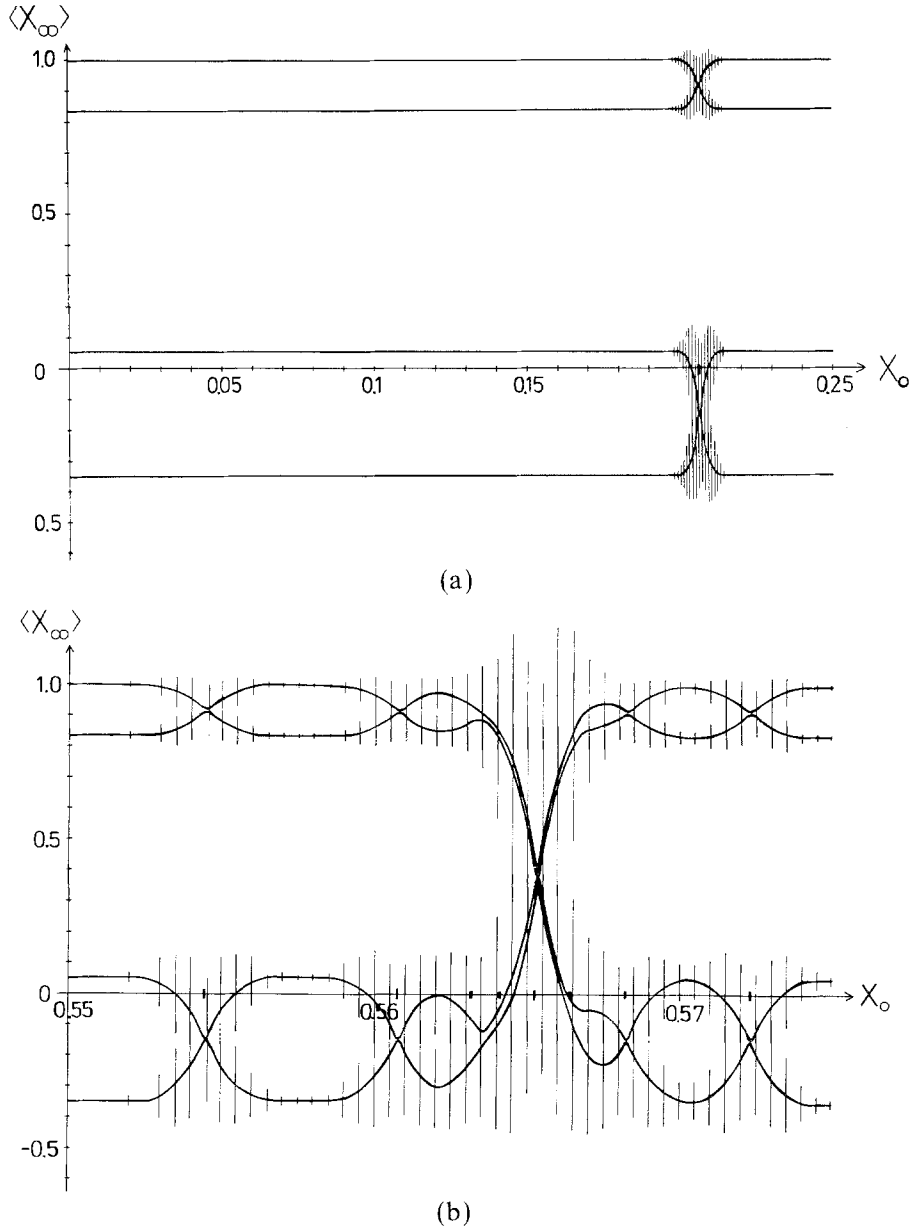

Fig. 2. The location of the average attractors $\langle x_\infty \rangle$ as a function of the starting point x_0 for $\mu = 1.36$ and $\sigma = 10^{-3}$: (a) $0 \leqslant x_0 \leqslant 0.25$, (b) $0.550 \leqslant x_0 \leqslant 0.575$. The vertical lines denote the values of the standard deviation from the average value. The points x_0^α are denoted by markers.

close to μ_c only periodic attractors with finite and not arbitrarily large periodicity are observed is also due to averaging over neighboring branches ($\mu < \mu_c$) or bands ($\mu > \mu_c$) which are separated by less then σ in the noiseless case. The bifurcation diagram for the average value reflects the existence of periodic windows within the chaotic regime of the noiseless map.[14] Though for reasons of clarity these windows are not displayed on Fig. 1, one finds for the relevant μ values average attractors with the appropriate window periodicity; the shifted attractors are also present in the window.

A characteristic property by which the average bifurcation diagram differs from the noiseless one is the location of the period-doubing transitions. In the average case this transition is shifted toward higher μ values as compared to the noiseless case. However, the precise numerical location of the period-doubling transition is hardly possible due to the critical slowing down which enlarges (up to infinity) the number of iterations necessary to reach equilibrium around those special μ points. Also, due to the critical slowing down one is not able to determine numerically whether the period doubling happens continuously (as in the noiseless case) or discontinuously (see the next section). For this reason , on Fig. 1 we leave this undecided.

Finally, Fig. 1 displays the behavior of the standard deviation as a function of μ. For ordinary starting points the standard deviation remains small (of order σ) for $\mu < \mu_c(\sigma)$. The only exceptions in this μ regime are the points of the period-doubling transitions where the standard deviation shows local, finite maxima.[5] It is, however, not possible to display them on the scale of Fig. 1. For $\mu > \mu_c(\sigma)$ the standard deviation does not remain small in the long-time limit; this long-time limit starts growing with increasing μ. We see that for large enough μ values the standard deviation is of order one. The critical value of the control parameter $\mu_c(\sigma)$ tends to μ_c for $\sigma \to 0$; for $\sigma \neq 0$ $\mu_c(\sigma) < \mu_c$. For the exceptional starting points the standard deviation does not remain small even for $\mu < \mu_c(\sigma)$ (Figs. 2a, b). This fact is not astonishing if one recalls the mechanism producing the shifted attractors. Thus because of the magnitude of the standard deviation the average value alone does not give a good characterization of the average dynamics neither for $\mu > \mu_c(\sigma)$ nor for the exceptional starting points.

3. AVERAGE EQUATION OF MOTION

In this section we derive a deterministic average equation of motion which describes in an approximate way the time evolution of the average value and of the variance. The starting point is the noisy map (1) and we

assume that the noise distribution is characterized by the single parameter σ. After averaging both sides of (1) over the noise distribution one gets:

$$\bar{x}_{n+1} = \overline{F(\bar{x}_n + \Delta_n)} = F(\bar{x}_n) + 0.5 \cdot F'' \cdot \overline{\Delta_n^2} \tag{2}$$

where $\Delta_n \equiv x_n - \bar{x}_n$ and $\bar{x}_0 = x_0$. Similarly

$$\Delta_{n+1} = F(x_n) - \bar{x}_{n+1} + \zeta_n = F'(\bar{x}_n) \cdot \Delta_n + \zeta_n + 0.5 \cdot F'' \cdot (\Delta_n^2 - \overline{\Delta_n^2})$$

and

$$\begin{aligned} \overline{\Delta_{n+1}^2} = {} & F'^2(\bar{x}_n) \cdot \overline{\Delta_n^2} + \overline{\zeta_n^2} + 0.25 \cdot F''^2 \cdot \overline{(\Delta_n^2 - \overline{\Delta_n^2})^2} + 2 \cdot F'(\bar{x}_n) \cdot \overline{\Delta_n \cdot \zeta_n} \\ & + F'' \cdot F'(\bar{x}_n) \cdot \overline{\Delta_n \cdot (\Delta_n^2 - \overline{\Delta_n^2})} + F'' \cdot \overline{(\Delta_n^2 - \overline{\Delta_n^2}) \cdot \zeta_n} \end{aligned} \tag{3}$$

Since it follows from causality that $\overline{\Delta_n \cdot \zeta_n} = 0$ for all $n \geqslant 0$ then

$$\overline{\Delta_{n+1}^2} = F'^2(\bar{x}_n) \cdot \overline{\Delta_n^2} + \sigma^2 + \text{higher order moments} \tag{4}$$

Neglecting the higher order moments in the small noise limit[15] and introducing $\bar{y}_n \equiv 0.5 \cdot F'' \cdot \overline{\Delta_n^2}$ one obtains the two-dimensional map

$$\begin{aligned} \bar{x}_{n+1} &= F(\bar{x}_n) + \bar{y}_n \\ \bar{y}_{n+1} &= F'^2(\bar{x}_n) \cdot \bar{y}_n + 0.5 \cdot F'' \cdot \sigma^2 \end{aligned} \tag{5}$$

with the initial condition $\bar{x}_0 = x_0$, $\bar{y}_0 = 0$.

Obviously, by putting $\sigma = 0$ (which implies $\bar{y}_n = 0$ for all $n \geqslant 0$) one recovers the one-dimensional deterministic equation $x_{n+1} = F(x_n)$. Equation (5) can be extended to cover also the case of the parametric (multiplicative) noise. By this we mean a situation in which the control parameter μ in Eq. (1) is replaced by a random variable $\mu_n = \bar{\mu} + \eta_n$ with $\bar{\eta}_n = 0$ and $\overline{\eta_n \eta_m} = \tau^2 \cdot \delta_{nm}$. If for simplicity we assume that the parametric and additive noises are uncorrelated, $\overline{\zeta_n \eta_m} = 0$, then in the limit $\sigma \ll 1$, $\tau \ll 1$ the average equation of motion takes again the form (5) with μ replaced by $\bar{\mu}$ and the noise strength σ replaced by an effective noise strength $(\sigma^2 + \tau^2 \cdot \bar{x}_n^4)^{0.5}$. Because $\bar{x}_n$ is a bounded quantity the effective noise strength is again small in the limit $\sigma \ll 1$, $\tau \ll 1$. The analysis of this more general case gives the same results as the analysis of Eq. (5), and so we restrict our discussion to the additive case only, Eq. (5).

The average equation of motion is approximate and the approximation leading to it assumes that the variance $\sim(-\bar{y}_n)$ remains small in the course of time. Numerical solutions of (5) fulfill this condition only for μ values below a certain critical one; above it the long-time behavior of the solutions of (5) is characterized by large variance and so

the validity of this map breaks down (this fact could of course be anticipated on the basis of the simulation presented in section 2). However, from the mathematical point of view the average equation has many unusual properties which make its analysis interesting independently from the original motivation.[6] Below we discuss these properties and compare them with the results of simulation.

The long-time behavior of the solutions of (5) depends on two parameters μ and σ and on the initial point x_0. Thus in order to classify the attractors of Eq. (5) one should use the five-dimensional space of variables $\mu, \sigma, x_0, \bar{x}_\infty, \bar{y}_\infty$. In the following we shall look at certain sections of this space in order to discuss separately the dependence of $\bar{x}_\infty$ and $\bar{y}_\infty$ on x_0, μ, and σ.

Basins of Attraction

We start with the dependence on x_0 and discuss the basins of attraction. We fix σ (e.g., $\sigma = 10^{-3}$) and take μ in the range corresponding to the period-doubling regime of the noiseless map. In this regime the average attractors are also periodic and undergo period-doubling transitions. The set of starting points $[-1, 1]$ is divided into subsegments in such a way that all points belonging to a given subsegment lead to the same attractor.[16] Division into different basins of attraction is shown on Figs. 3a, b which should be compared with analogous results from simulation, Figs. 2a, b. The attractors shown on this picture are numbered III, II′, I′ and just as in the simulation most of the starting points lead to the long-time behavior described by attractor III with period 4. Its location agrees up to order $O(\sigma^2)$ with the location of the corresponding attractor in the noise-free case, and for this reason we call it the ordinary attractor. The other two attractors, II′ and I′, have small but nonzero basins of attraction. We call them the exceptional attractors and according to map (5) they take the role of the shifted attractors from simulation. The division into basins of attraction depends on the values of μ and σ and becomes finer when μ is increased toward μ_c at fixed σ. On the other hand, when μ is kept fixed and σ becomes smaller the basins of attraction for the exceptional attractors shrink and their total length goes to zero in the limit $\sigma \to 0$.

The value of the standard deviation depends significantly on whether one considers the ordinary or the exceptional attractors. For ordinary starting points the standard deviation remains small, of order σ, in the course of time. For the exceptional starting points the standard deviation remains finite, but grows in time up to order 1. As an example, Figs. 3a, b show the behavior of the standard deviation as function of x_0 at fixed μ

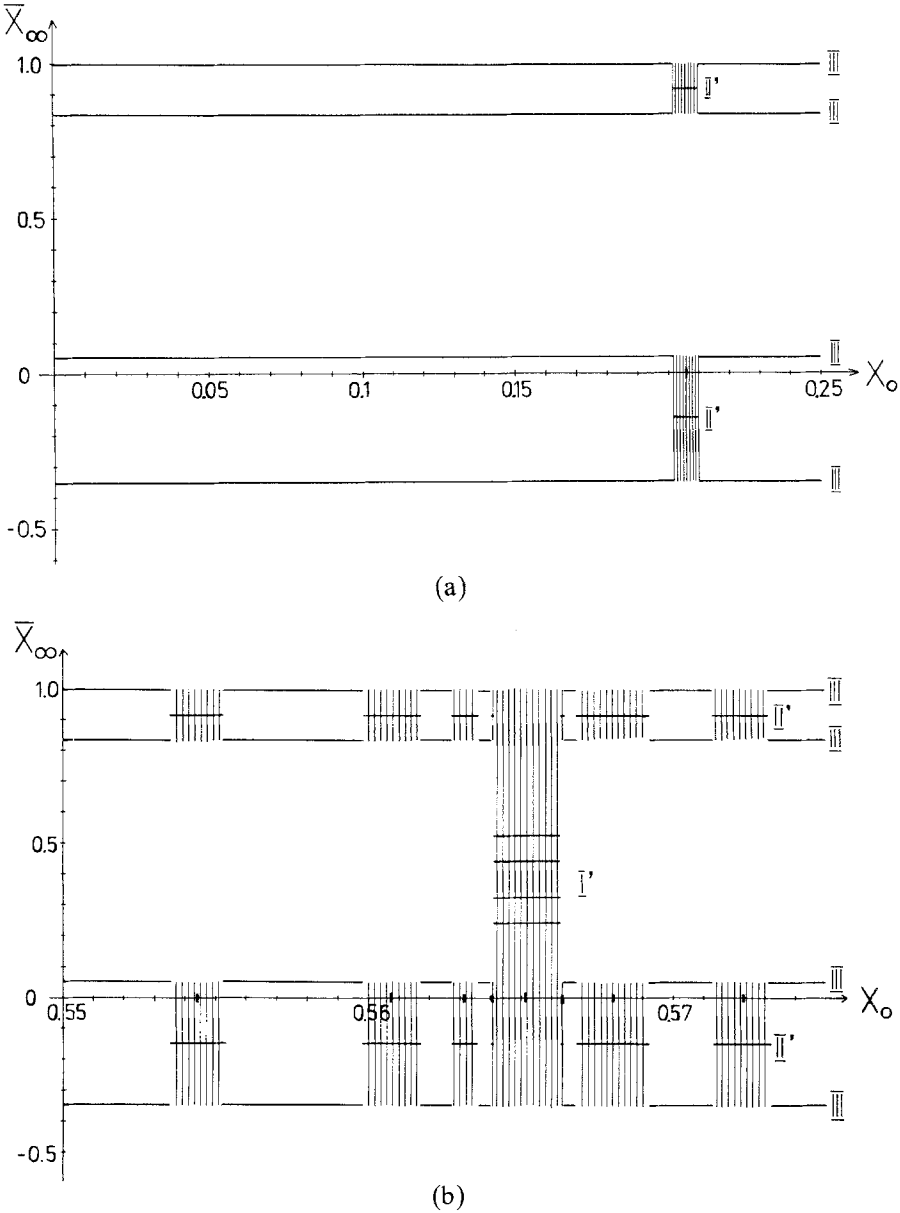

Fig. 3. The basins of attraction obtained from the map (5) for $\mu = 1.36$ and $\sigma = 10^{-3}$: (a) $0 \leqslant x_0 \leqslant 0.25$, (b) $0.550 \leqslant x_0 \leqslant 0.575$. Most of the starting points lead to the ordinary period-4 attractor III; the rest lead to the exceptional period-2 attractor II′ and period-4 attractor I′. As on Fig. 2, the vertical lines denote the value of the standard deviation calculated from map (5). Markers denote the points x_0^α.

and σ. The division of starting points into basins of attraction persists also in the μ regime where both the ordinary and the exceptional attractors become chaotic (the transition to chaos as predicted by the map (5) is discussed in the next section). This division depends again on both μ and σ and becomes less and less fine when we increase μ at fixed σ. Finally, for large enough μ there exists only one basin of attraction leading to the unique chaotic attractor.

Within the chaotic regime there are periodic windows located similarly to the noiseless case. At each periodic window there are both ordinary and exceptional attractors present, each of them having a different basin of attraction. There is, however, one important difference as compared to the situation shown on Figs. 3a, b. At a periodic window located at high μ values the ordinary attractors are no longer obtained from the overwhelming majority of starting points. This change becomes obvious when one looks back at the mechanism producing the exceptional attractors. The noiseless map at large μ values is characterized by the existence of many points x_0^x and they are located close to each other; when μ grows these points fill the J segment more and more densely. Since the basins of the exceptional attractors are centered just at points x_0^x nearly all the starting points—for appropriately large μ values and not too small noise strength σ—lead to the exceptional attractors.

The Transition to Chaos

The schematic bifurcation diagram for noise strength $\sigma = 10^{-3}$ is shown in Fig. 4 where heavy lines denote the ordinary attractors I, II, III, IV and thin lines denote the exceptional attractors I′, II′, III′. We first discuss the exceptional attractors. As μ increases the evolution of each of them is similar and as an example we concentrate on the exceptional attractor I'. It continues the ordinary attractor I and so initially has periodicity 1. When further increasing μ it undergoes a period-quadrupling transition[17] which is then followed by an infinite sequence of period doublings to chaos. Only the first of those period-doubling transitions is displayed on Fig. 4. The attractors II′ and III′ behave in the same way. Thus the exceptional attractors undergo the Feigenbaum scenario.[8,9] The Feigenbaum constant δ calculated up to period 2^{11} is $\delta = 4.669$.

On the ordinary attractors the route to chaos is different. They undergo a finite number of discontinuous period-doubling transitions before the chaos sets in. These discontinuous period doublings are located at μ values which are bigger than the corresponding values for the noiseless case (see Table I). As already remarked, the origin of the shift can be explained on the basis of the noisy equation (1) in a similar way as the

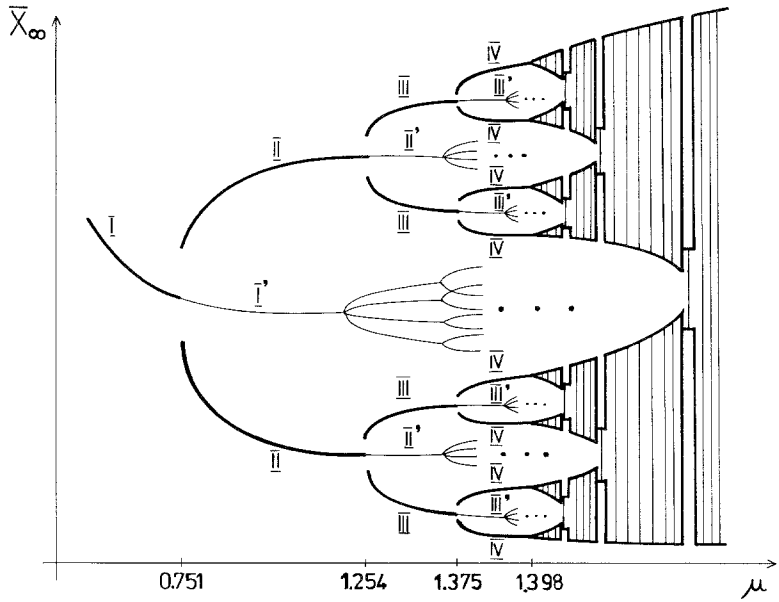

Fig. 4. Schematic bifurcation diagram from map (5) for $\sigma = 10^{-3}$. The ordinary attractors I–IV are displayed in heavy lines and the exceptional attractors I′–III′ in thin lines.

origin of the exceptional attractors. Mathematically this discontinuous period doubling is caused by a mechanism similar to tangent bifurcation,[18,19] (Fig. 6). After a finite number of discontinuous period doublings chaos sets in. The periodicity of the ordinary attractor becoming chaotic depends on noise strength and, for example, is equal to 8 for $\sigma = 10^{-3}$, 16 for $\sigma = 10^{-4}$, 32 for $\sigma = 10^{-5}$. The scenario for the onset of chaos can be best illustrated in the $\bar{x}\bar{y}$ plane of the two-dimensional map (5) and is as follows: First there is a Hopf bifurcation[20] at which a periodic attractor becomes quasi-periodic. This means that in the $\bar{x}\bar{y}$ plane

Table I. Comparison Between Noiseless Case and Discontinuous Period Doublings for Different Noise Strengths

	$\sigma = 0$	$\sigma = 10^{-4}$	$\sigma = 10^{-3}$	$\sigma = 10^{-2}$
$\mu_{1\to 2}$	0.7500	0.7501	0.7514	0.7655
$\mu_{2\to 4}$	1.2500	1.2504	1.2540	1.2981
$\mu_{4\to 8}$	1.3681	1.3688	1.3751	—
$\mu_{8\to 16}$	1.3940	1.3950	—	—

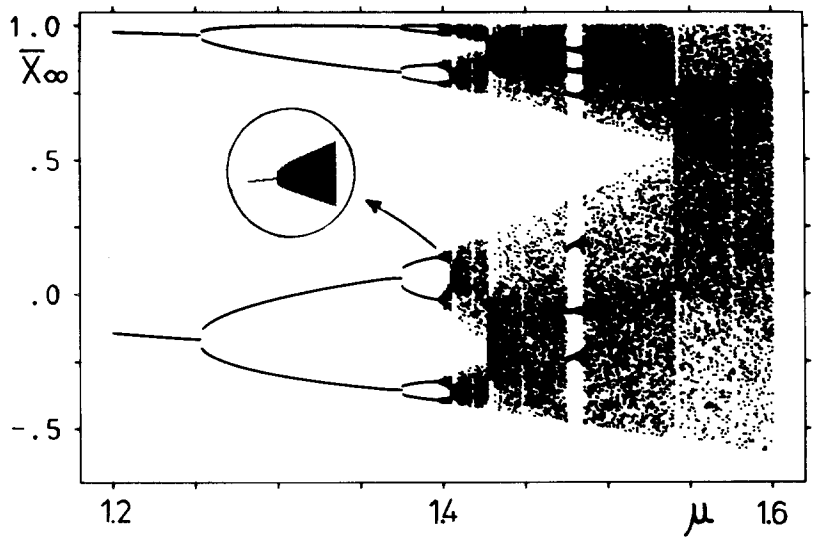

Fig. 5. The numerical bifurcation diagram from map (5) for $\sigma = 10^{-3}$. In the subharmonic regime only the ordinary attractors are shown. In the window around $\mu = 1.48$ both ordinary and exceptional attractors are present but only the latter is shown. The inset contains the enlargement of the Hopf bifurcation, which for this noise strength takes place after three discontinuous period doublings.

a set of q points representing the period-q attractor turnes into a set of q closed curves representing the quasi-periodic attractor. On the bifurcation diagram (Figs. 4, 5) the Hopf bifurcation corresponds to the line broadening of the ordinary attractor. Upon further increasing of μ each of these q curves changes its shape (remaining a closed curve) until at certain μ value it turns into a set of points. This is again a periodic solution which persists for some interval of μ values until it turns again into a quasi-periodic solution; in the $\bar{x}\bar{y}$ plane it is again represented by a set of q closed curves.

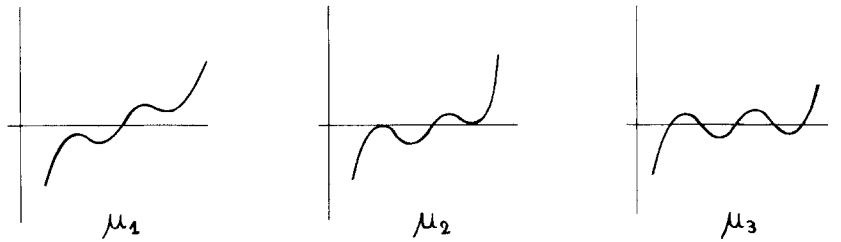

Fig. 6. The schematic tangent bifurcation responsible for the discontinuous period-doubling transition. On the vertical axis we plot the function of x, which zeroes represent the fixed points of the second iterate of map (5). This function is obtained by iterating map (5) once, equating $\bar{x}'' = \bar{x}$, $\bar{y}'' = \bar{y}$, and eliminating the variable $\bar{y}$. At $\mu = \mu_2$ ($\mu_1 < \mu_2 < \mu_3$) the discontinuous period doubling takes place.

This sequence of transitions from quasi-periodic attractors to periodic and again to quasi-periodic as μ increases is repeated a number of times. Each time the periodic attractor has different periodicity but the quasi-periodic one always consists of q curves. Finally a periodic attractor turns into a chaotic attractor.[21,22]

In the $\bar{x}\bar{y}$ plane this corresponds to a set of points turning into a strange attractor consisting of q subsets. The above scenario for the transition to chaos via the Hopf bifurcation is well illustrated by the behavior of the Liapunov exponent[16,23] as a function of μ. The Liapunov exponent is negative on periodic attractors, zero on quasi-periodic attractors and positive on strange attractors (Fig. 7). The number of periodic windows in the quasi-periodic regime depends on the noise strength but qualitatively the above picture holds for any nonzero noise. As one can see from the bifurcation diagram, Fig. 4, the onset of chaos is shifted toward smaller values of μ as compared to the noiseless case.

On the chaotic side of the bifurcation diagram the phenomenon of discontinuous band mergings is observed. Though on the numerical bifurcation diagram, Fig. 5, the band mergings look similar to the noiseless case, a closer examination reveals that the details behind are quite different. In fact the band mergings proceed via crises[24,25] and this is schematically displayed on Fig. 8. The unstable periodic orbit (dashed line) which is produced together with the ordinary attractor (heavy line) at the discontinuous bifurcation collides for larger μ values with this ordinary attractor which has already turned chaotic; on Fig. 8 the unstable orbit III″ collides

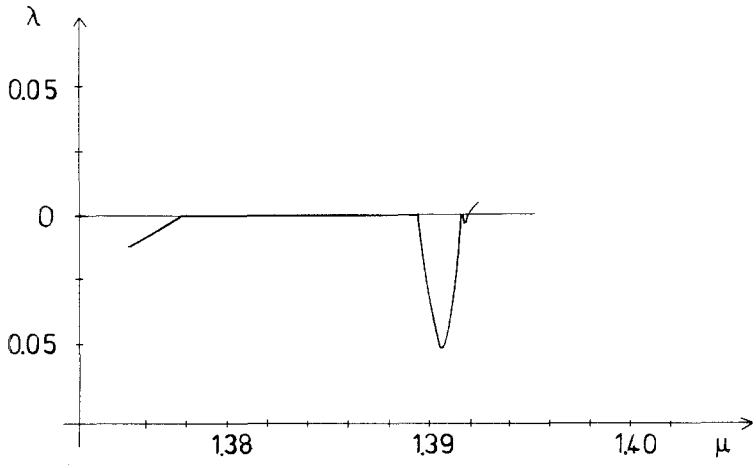

Fig. 7. The behavior of the Liapunov exponent as a function of μ at the transition to chaos via the Hopf bifurcation for $\sigma = 10^{-2}$.

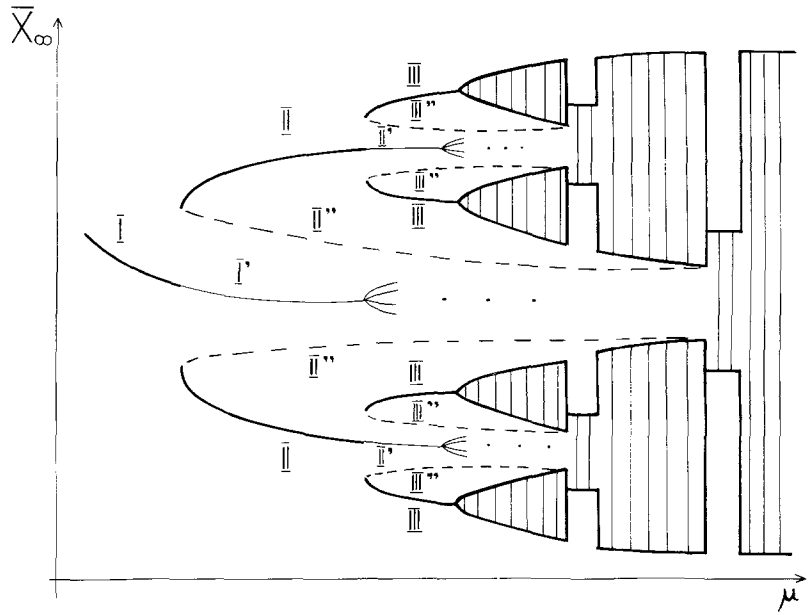

Fig. 8. Schematic bifurcation diagram for $\sigma = 10^{-2}$ showing the disappearance and broadening of chaotic attractors via crises. The dashed lines denote the unstable periodic orbits.

with chaotic attractor III. As a result the chaotic ordinary attractor disappears and only the chaotic attractor II′ remains; this is the narrow part of the bifurcation diagram. The above mechanism of chaotic attractor vanishing is called the external crisis.[24] For slightly larger μ values this remaining chaotic attractor suddenly broadens up (via internal crisis[24]) and continues until it collides again with another unstable orbit, II″ on Fig. 8. This external crisis leads again to the disappearance of the chaotic attractor II′ after which only the exceptional chaotic attractor I′ remains. I′ in turn undergoes internal crisis, causing its sudden broadening. For μ values slightly larger than those corresponding to the external crises one observes also the phenomenon of transient chaos.[24]

The bifurcation diagram for the variance, similarly to the average value, shows the transition to chaos. On the ordinary attractors the variance undergoes a finite number of discontinuous period doublings before chaos sets in via the Hopf bifurcation (Fig. 9). On the exceptional attractors one observes the Feigenbaum scenario preceded by the period quadrupling. For those μ values for which the average attractor consists of bands, the attractor for the variance also consists of bands. The lower limit of each variance band is located around zero. The upper limit which gives the maximum value of variance on a given band depends significantly on μ.

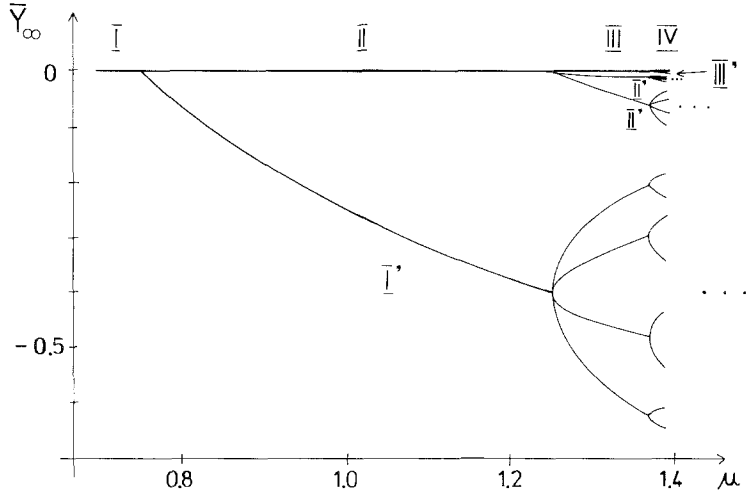

Fig. 9. Bifurcation diagram for the variable $\bar{y}_\infty = -\mu \cdot \overline{\Delta_\infty^2}$ for $\sigma = 10^{-3}$. Only on the ordinary attractors I–IV in the periodic regime the variance remains small $[O(\sigma^2)]$. Due to the large scale of this picture it is not possible to display either the periodic structure of the attractors II–IV or the local maxima around the period doublings.

The upper limit is small (of order $O(\sigma^2)$) for μ close to the location of the Hopf bifurcation and starts growing up to order 1 upon increasing μ. In this sense the results from the map (5) agree with the predictions of the simulation, though of course in the simulation neither the average value nor the variance show any chaotic behavior. As already noted the variance is large on the exceptional attractors in the periodic regime; in the sense described above it also remains large on the chaotic exceptional attractors.

The two-dimensional map (5) predicts the existence of the bifurcation gap. The finite number of period-doubling transitions predicted by this map agrees with the results of computer simulation. Also the shift of the period-doubling transitions as compared with the noiseless case is obtained from both the simulation and the map. However, beyond the Hopf bifurcation the validity of map (5) breaks down and for those μ values where the simulation predicts periodic attractors map (5) gives chaotic attractors consisting of bands. On the other hand the order of magnitude of the standard deviation as obtained from simulation agrees with the upper limit of the standard deviation calculated from map (5).

4. SCALING PROPERTIES OF $\bar{x}_n$ AND $\overline{\Delta_n^2}$

The average value $\bar{x}_n$ and the variance $\overline{\Delta_n^2}$ show scaling properties[26] with respect to parameters μ, σ, starting point x_0, and time n. These

properties can be obtained either directly from the map (5) or from the path integral formulation of the problem.[3] The latter approach was used previously to discuss the scaling of the Liapunov exponent[2,3] and it is used first in the present context. In this method one starts from a generalized version of the noisy equation (1)

$$x_{n+1} = f_\mu(x_n; m) + \zeta_n \cdot g_\mu(x_n; m) \tag{6}$$

where

$$f_\mu(x; m) = (\underbrace{F \circ F \circ \cdots \circ F}_{m \text{ times}})(x) \tag{7}$$

and the function $g_\mu(x; m)$ guarantees that Eq. (6) does not change its form after one iteration. With the gaussian probability distribution for the noise, the average value is calculated from the following path integral[3]

$$\bar{x}_n(\mu, \sigma; x_0) = \int Dx \int Ds \cdot x_n \cdot \exp\left[\sum_{p=0} \{is_p(x_{p+1} - f_\mu(x_p; m)) - 0.5 \cdot \sigma^2 \cdot s_p^2 \cdot g_\mu^2(x_p; m)\}\right] \tag{8}$$

where $\int Dx \equiv \int dx_1 \ldots \int dx_k \ldots$ and $\int Ds \equiv (2\pi)^{-1} \int ds_0 \ldots (2\pi)^{-1} \int ds_k \ldots$. Using the saddle point method we integrate over every s_p with even p and every x_p with odd p (n is assumed to be even) and then put the result back into the form (8)

$$\bar{x}_n(\mu, \sigma; x_0) = \int Dx \int Ds \cdot x_n \cdot \exp\left[\sum_{\text{odd } p} \{is_p(x_{p+1} - \tilde{f}_\mu(x_{p-1}; m)) - 0.5 \cdot \sigma^2 \cdot s_p^2 \cdot \tilde{g}_\mu^2(x_{p-1}; m)\}\right] \tag{9}$$

where

$$\tilde{f}_\mu(x; m) = f_\mu[f_\mu(x; m); m] + 0.5 \cdot \sigma^2 \cdot g_\mu^2(x; m) \cdot f''_\mu[f_\mu(x; m); m] \tag{10a}$$

$$\tilde{g}_\mu^2(x; m) = g_\mu^2[f_\mu(x; m); m] + g_\mu^2(x; m) \cdot f'^2_\mu[f_\mu(x; m); m] \tag{10b}$$

and now $\int Dx \equiv \int dx_2 \ldots \int dx_{2k} \ldots$ and $\int Ds = (2\pi)^{-1} \int ds_1 \ldots (2\pi)^{-1} \int ds_{2k+1} \ldots$. The origin of the term proportional to σ^2 on the RHS of Eq. (10a) is different than the origin of the first term which results from the change of the integration variables in (8). The second term comes from expanding the argument of the exponential function $\exp[0.5 \cdot i \cdot \arctan$

$\{s \cdot \sigma^2 \cdot g_\mu^2(x; m) \cdot f''_\mu[f_\mu(x; m); m]\}]$ (obtained from integration over s and x) in powers of σ^2 and keeping only terms linear in s. If in the limit $\sigma \ll 1$ one neglects the second term in (10a) in comparison with the first (as Shrayman et al.[3] do), then rescales the variables

$$s_{2k+1} = -\alpha s'_k \qquad x_{2k} = (-\alpha)^{-1} x'_k \tag{11}$$

and uses the scaling properties of functions $\tilde{f}_\mu$ and $\tilde{g}_\mu$[3,8]

$$\begin{aligned} \tilde{f}_{\mu_k}(x; m) &= (-\alpha)^{-1} \cdot f_{\mu_{k-1}}(-\alpha x; m) \\ \tilde{g}^2_{\mu_k}(x; m) &= \beta^2 \cdot \alpha^{-2} \cdot g^2_{\mu_{k-1}}(-\alpha x; m) \end{aligned} \tag{12}$$

one finally obtains

$$\bar{x}_{2n}(\mu_{k+1}, \sigma; x_0) = (-\alpha)^{-1} \cdot \bar{x}_n(\mu_k, \beta\sigma, -\alpha x_0) \tag{13}$$

μ_k and μ_{k-1} denote the points with corresponding stability for 2^k and 2^{k-1} periodic attractors, respectively, and $\alpha = 2.503$, $\beta = 6.619$. After introducing the variable $\varepsilon = \mu_c - \mu$ formula (13) takes the scaling form

$$\bar{x}_{2n}(\varepsilon, \sigma, x_0) = (-\alpha)^{-1} \cdot \bar{x}_n(\varepsilon\delta, \sigma\beta, -\alpha x_0) \tag{14}$$

Similarly one obtains for the variance

$$\overline{\Delta^2_{2n}}(\varepsilon, \sigma, x_0) = \alpha^{-2} \cdot \overline{\Delta^2_n}(\varepsilon\delta, \sigma\beta; -\alpha x_0) \tag{15}$$

The scaling formulas (14, 15) can also be obtained from the two-dimensional map (5). In this case, however, this map has to be rederived for the case in which the noisy equation has the general form (6). The derivation goes exactly the same way as for Eq. (5), and one obtains

$$\begin{aligned} \bar{x}_{n+1} &= f_{\mu_k}(\bar{x}_n; m) + 0.5 \cdot f''_{\mu_k}(\bar{x}_n; m) \cdot \overline{\Delta^2_n} \\ \overline{\Delta^2_{n+1}} &= f'^2_{\mu_k}(\bar{x}_n; m) \cdot \overline{\Delta^2_n} + g^2_{\mu_k}(\bar{x}_n; m) \cdot \sigma^2 \end{aligned} \tag{16}$$

By iterating Eq. (16) once and retaining terms up to order σ^2 one obtains

$$\begin{aligned} \bar{x}_{n+2} &= f_{\mu_k}[f_{\mu_k}(\bar{x}_n; m); m] + 0.5\sigma^2 \cdot g^2_{\mu_k}(\bar{x}_n; m) \cdot f''_{\mu_k}[f_{\mu_k}(\bar{x}_n; m); m] \\ &\quad + 0.5 \cdot \overline{\Delta^2_n}[f''_{\mu_k}[f_{\mu_k}(\bar{x}_n; m); m] \cdot f'^2_{\mu_k}(\bar{x}_n; m) \\ &\quad + f'_{\mu_k}[f_{\mu_k}(\bar{x}_n; m); m] \cdot f''_{\mu_k}(\bar{x}_n; m)] \\ \overline{\Delta^2_{n+2}} &= f'^2_{\mu_k}[f_{\mu_k}(\bar{x}_n; m); m] \cdot f'^2_{\mu_k}(\bar{x}_n; m) \cdot \overline{\Delta^2_n} \\ &\quad + \sigma^2 \cdot \{g^2_{\mu_k}[f_{\mu_k}(\bar{x}_n; m); m] + g^2_{\mu_k}(\bar{x}_n; m) \cdot f'^2_{\mu_k}[f_{\mu_k}(\bar{x}_n; m); m]\} \end{aligned} \tag{17}$$

We see that functions $\tilde{f}_\mu$ and $\tilde{g}_\mu$ defined in Eqs. (10a) and (10b) appear on the RHS of Eqs. (17), which can thus be rewritten as

$$\begin{aligned} \bar{x}_{n+2} &= \tilde{f}_{\mu_k}(\bar{x}_n; m) + 0.5 \cdot \tilde{f}''_{\mu_k}(\bar{x}_n; m) \cdot \overline{\Delta_n^2} \\ \overline{\Delta_{n+2}^2} &= \tilde{f}'^2_{\mu_k}(\bar{x}_n; m) \cdot \overline{\Delta_n^2} + \sigma^2 \cdot \tilde{g}^2_{\mu_k}(\bar{x}_n; m) \end{aligned} \tag{18}$$

After making the same truncation in Eq. (10a) as previously and using the scaling properties (12), Eqs. (18) take the form

$$\begin{aligned} -\alpha \bar{x}_{n+2} &= f_{\mu_{k-1}}(-\alpha \bar{x}_n; m) + 0.5 \cdot f''_{\mu_{k-1}}(-\alpha \bar{x}_n; m) \cdot \alpha \cdot \overline{\Delta_n^2} \\ \alpha^2 \overline{\Delta_{n+2}^2} &= f'^2_{\mu_{k-1}}(-\alpha x_n; m) \cdot \alpha^2 \cdot \overline{\Delta_n^2} + \sigma^2 \cdot \beta^2 \cdot g^2_{\mu_{k-1}}(-\alpha x_n; m) \end{aligned} \tag{19}$$

From comparing Eqs. (19) and (16) we see that the average value $\bar{x}_n$ and the variance $\overline{\Delta_n^2}$ fulfill the scaling relations (14, 15). These scaling properties can be used to locate the borderline of the bifurcation gap.[26]

The variance can be looked upon as the analog of the order parameter from the critical phenomena physics. We fix the parameter ε at a value which corresponds in the noiseless case either to periodic attractor with periodicity k ($\varepsilon > 0$) or to chaotic attractor consisting of k separate bands ($\varepsilon < 0$) and we consider the double limit:

$$\chi_k(\varepsilon) = \lim_{\sigma \to 0} \lim_{n \to \infty} \overline{\Delta_{n \cdot k}^2}(\varepsilon, \sigma; 0)$$

(for simplicity we take $x_0 = 0$). The value of this double limit is different for the periodic and chaotic case[26]

$$\chi_k(\varepsilon) \begin{cases} = 0 & \text{for } \varepsilon > 0 \\ \neq 0 & \text{for } \varepsilon < 0 \end{cases} \tag{20}$$

It follows from the scaling relation (15) that the long-time limit of the variance $\overline{\Delta^2}(\varepsilon, \sigma) \equiv \overline{\Delta_\infty^2}(\varepsilon, \sigma; 0)$ has the scaling form

$$\Delta^2(\varepsilon, \sigma) = \sigma^{2(\ln \alpha / \ln \beta)} \cdot \Psi\left(\frac{\varepsilon \cdot \phi_1(\ln \varepsilon)}{\sigma^{\ln \delta / \ln \beta} \cdot \phi_2(\ln \sigma)} \right) \cdot \phi_3(\ln \sigma) \tag{21}$$

where $\phi_{1,2,3}$ are periodic functions $\phi_1(x + \ln \delta) = \phi_1(x)$, $\phi_{2,3}(x + \ln \beta) = \phi_{2,3}(x)$. Equation (21) implies the following asymptotic behavior of $\Delta^2(0, \sigma)$ in the limit $\sigma \to 0$

$$\Delta^2(0, \sigma) \sim \sigma^{2(\ln \alpha / \ln \beta)} = \sigma^{0.97} \tag{22}$$

Equations (20, 22) show that the variance behaves analogously to the order parameter from the critical phenomena while the noise strength σ takes the role of the ordering field.

5. CONCLUSIONS

The structure of attractors characterizing the long-time limit of the average dynamics is in many respects different from the corresponding noiseless case. The results of computer simulation show that the bifurcation diagram for the average value displays only periodic attractors with certain symmetry between large and small values of the control parameter. For a fixed value of noise strength a finite number of period-doubling transitions is observed after which an inverse process of mergings of the branches of the periodic attractors follows. However, the symmetry between the large and small values of the control parameter is broken if together with the average value also the standard deviation from the average value is analyzed. This standard deviation is small for lower μ values and becomes large for higher μ values. This property of standard deviation makes the problem of average dynamics difficult to describe analytically. The approximate two-dimensional map analyzed in this paper ceases to give the proper description of the average dynamics just at those μ values where the inverse cascade of mergings starts. However, the interesting property of the two-dimensional map is that it predicts a finite number of period-doubling transitions. After that the branches of the periodic attractors start to form bands which then undergo the inverse cascade of discontinuous mergings. The number of bands obtained from the map for given μ and σ agrees with the number of branches of the periodic attractors from the simulation. Finally, we mention that inclusion of higher order terms in the average equation of motion does not bring new results. Higher order moments can be included via an iterative approximation which leads to a three-dimensional map. However, no significant change in the long-time behavior was found in comparison with the two-dimensional map discussed in the text.

After this paper was finished, the authors were informed that a rigorous analysis of small random perturbation of the Feigenbaum map is given in Ref. 27.

ACKNOWLEDGMENT

The authors thank Professor Herbert Wagner for stimulating discussions and for his critical reading of the manuscript. Many valuable comments from Professor Herbert Spohn, and his constant interest in this work, are gratefully acknowledged. One of the authors (M.N.) acknowledges with pleasure the receipt of the Alexander von Humboldt fellowship.

REFERENCES

1. J. P. Crutchfield and B. A. Huberman, *Phys. Lett.* **77A**:407 (1980).
2. J. P. Crutchfield, M. Nauenberg, and J. Rudnick, *Phys. Rev. Lett.* **46**:933 (1981).
3. B. Shraiman, C. E. Wayne, and P. C. Martin, *Phys. Rev. Lett.* **46**:935 (1981).
4. J. P. Crutchfield, J. D. Farmer, and B. A. Huberman, *Phys. Rep.* **92**:45 (1982).
5. J. Heldstab, H. Thomas, T. Geisel, and G. Radons, *Z. Phys.* **B50:141** (1983); T. Geisel, J. Heldstab, and H. Thomas, *Z. Phys.* **B55:165** (1984).
6. R. Vallée, C. Delisle, and J. Chrostowski, *Phys. Rev.* **A30**:336 (1984).
7. G. Mayer-Kress and H. Haken, *J. Stat. Phys.* **26**:149 (1981).
8. M. Feigenbaum, *J. Stat. Phys.* **21**:669 (1979).
9. S. Grossman and S. Thomae, *Z. Naturforsch.* **32a**:1353 (1977).
10. M. Giglio, S. Musazzi, and U. Perini, *Phys. Rev. Lett.* **47**:243 (1981).
11. C. W. Smith, M. J. Tejwani, and D. A. Farris, *Phys. Rev. Lett.* **48**:492 (1982).
12. R. H. Simoyi, A. Wolf, and H. L. Swinney, *Phys. Rev. Lett.* **49**:245 (1982).
13. A. Libchaber, C. Laroche, and S. Fauve, *J. Physique Lett.* **43**:L211 (1982).
14. P. Collet, and J.-P. Eckmann, *Iterated Maps on the Interval as Dynamical Systems* (Birkhäuser, Boston, 1980).
15. The restriction to small noise ensures that the fraction of trajectories which leave the interval J is negligible. In analogy with critical phenomena the expansion (4) can be expected to break down at the bifurcation points of the noiseless map but we do not concentrate on this aspect in the present paper.
16. T. Hogg and B. A. Huberman, *Phys. Rev.* **A29**:275 (1984).
17. T. Janssen and J. A. Tjon, *Phys. Lett.* **87A**:139 (1982); *J. Phys.* **A16**:673, 697 (1983).
18. P. Manneville and Y. Pomeau, *Phys. Lett.* **75A**:1 (1979).
19. J. E. Hirsch, B. A. Huberman, and D. J. Scalapino, *Phys. Rev.* **A25**:519 (1982).
20. J.-P. Eckmann, *Rev. Mod. Phys.* **53**:643 (1981).
21. M. H. Jensen, P. Bak, and T. Bohr, *Phys. Rev.* **A30**:1960 (1984).
22. J. H. Curry, and J. A. Yorke in *The Structure of Attractors In Dynamical Systems*, N. G. Markley, J. C. Martin, and W. Perozo eds., Lecture Notes in Mathematics (Springer, Berlin, 1978), Vol. 668, 48.
23. S. D. Feit, *Comm. Math. Phys.* **61**:249 (1978).
24. G. Grebogi, E. Ott, and J. A. Yorke, *Phys. Rev. Lett.* **48**:1507 (1982); *Physica* **7D**:181 (1983).
25. Y. Gu, M. Tung, J.-M. Yuan, D. H. Feng, and M. M. Narducci, *Phys. Rev. Lett.* **52**:701 (1984).
26. M. Napiórkowski, *Phys. Lett.* **112A**:357 (1985).
27. F. B. Vul, Ya, G. Sinai, and K. M. Khanin, *Uspekhi Mat. Nauk* **39**(3):3 (1984) [*Russian Math. Surveys* **39**(3):1 (1984)].